

Supporting Information: Supplementary Figures

In-cell Detection of Conformational Sub-states of a GPCR Quaternary Structure: Modulation of Sub-state Probability by Cognate Ligand Binding

Joel Paprocki¹, Gabriel Biener¹, Michael Stoneman¹, Valerica Raicu^{1,2,*}

¹Department of Physics, ²Department of Biological Sciences, University of Wisconsin-Milwaukee, Wisconsin, USA

*Corresponding author: vraicu@uwm.edu

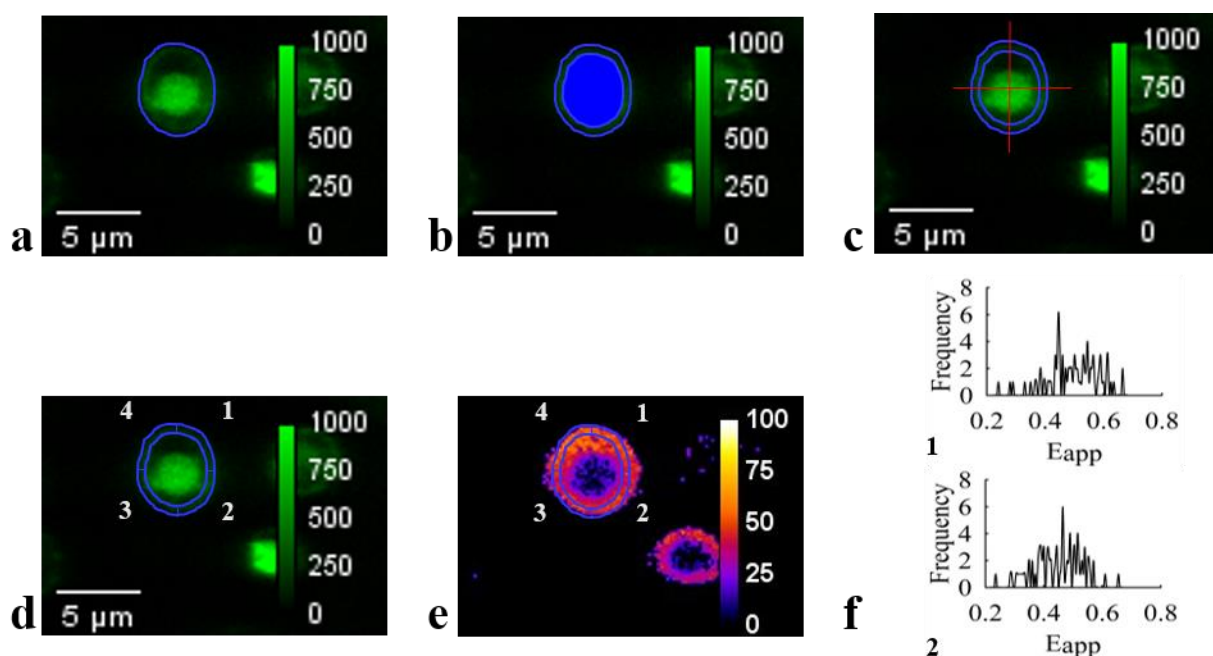


Figure S1. Isolation and segmentation of cell membrane micro-photographs. (a) k^{DA} image overlaid with a hand-drawn polygon (blue contour). (b) Computer-generated binary mask (blue solid area) overlaid on top of the image presented in panel a. All pixels within the hand-drawn, or outer, polygon which were more than 10 pixels from the closest point on the polygon were included in the mask. The exterior boundaries of the binary mask were used to create a second, or inner, polygon; the gap between the outer and inner polygon was 10 pixels. (c) The ring formed by the outer and inner polygons (two blue contours) was further divided into four segments by projecting lines outward from the center of mass every 90 degrees. (d) Display of the four generated segments (labeled 1-4). (e) The membrane segments were overlaid onto the pixel-level spatial E_{app} map obtained as described in the main body of the paper. (f) Examples of E_{app} histograms obtained from segments 1 and 2 in panel e.

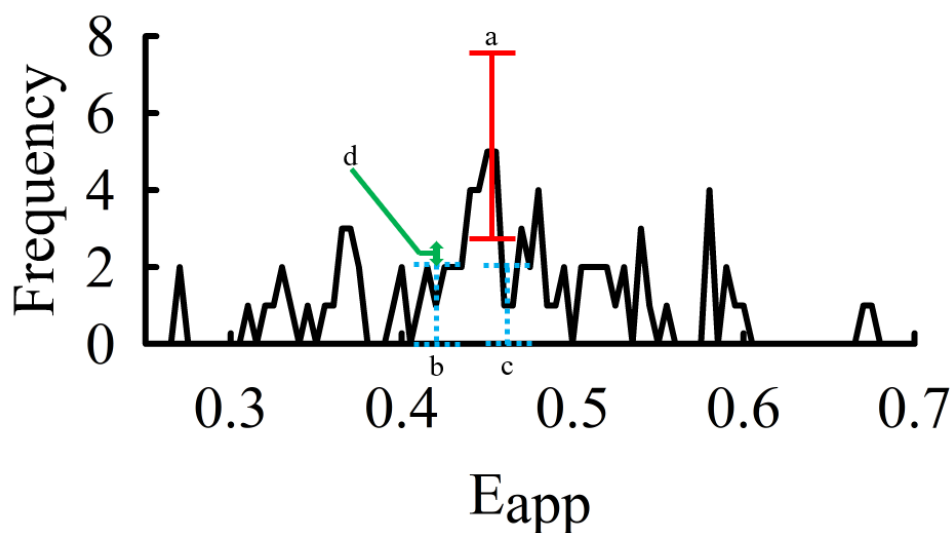


Figure S2. E_{app} histogram peak selection routine. E_{app} histogram (solid black line) was compiled from pixels enclosed within a single membrane segment. The peak selection routine was applied to extract a single predominant peak value. Location of a candidate peak, i.e., the E_{app} value corresponding to the highest frequency value, is shown with the vertical solid red line (labeled “a”). Nearby minima located to the left (“b”, frequency = 1) and right (“c”, frequency = 1) of the candidate peak are indicated by vertical dashed blue lines. The standard deviation of the E_{app} frequency value for the maximum (σ_{max}) and two minima (σ_{min}) locations are calculated by taking the square root of the corresponding frequency values. The horizontal solid red error bars indicate the range of uncertainty for the peak frequency value, which is calculated by taking the maximum peak frequency value $\pm \sigma_{max}$. Likewise, the horizontal dashed blue lines indicate the range of uncertainty for the neighboring minima, calculated by minimum frequency value $\pm \sigma_{min}$. For a candidate peak to be selected and used for further analysis, there must be no overlap between the error bars of the selected peak and the neighboring minima. For the particular candidate peak denoted by “a” there is a gap (green arrows labeled with “d”) between the lower end of the selected peak range and upper end of the minimum range, meaning this particular peak passed the peak selection criterion. If the gap for a candidate peak is less than or equal to zero, the peak is rejected and not used in compiling the meta-histogram.

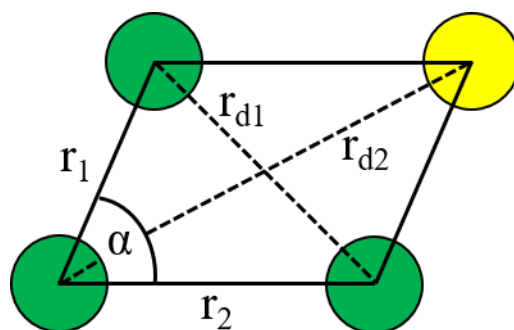


Figure S3. Example of a general parallelogram-shaped tetramer oligomer consisting of three donor- and one acceptor-labeled protomers. Green and yellow circles represent donor and acceptor fluorescent proteins, respectively. The various FRET efficiency values arising from different configurations of the parallelogram are dependent on the side lengths r_1 and r_2 as well as the acute angle, α . These three parameters completely determine the distances along the two diagonals, r_{d1} and r_{d2} .

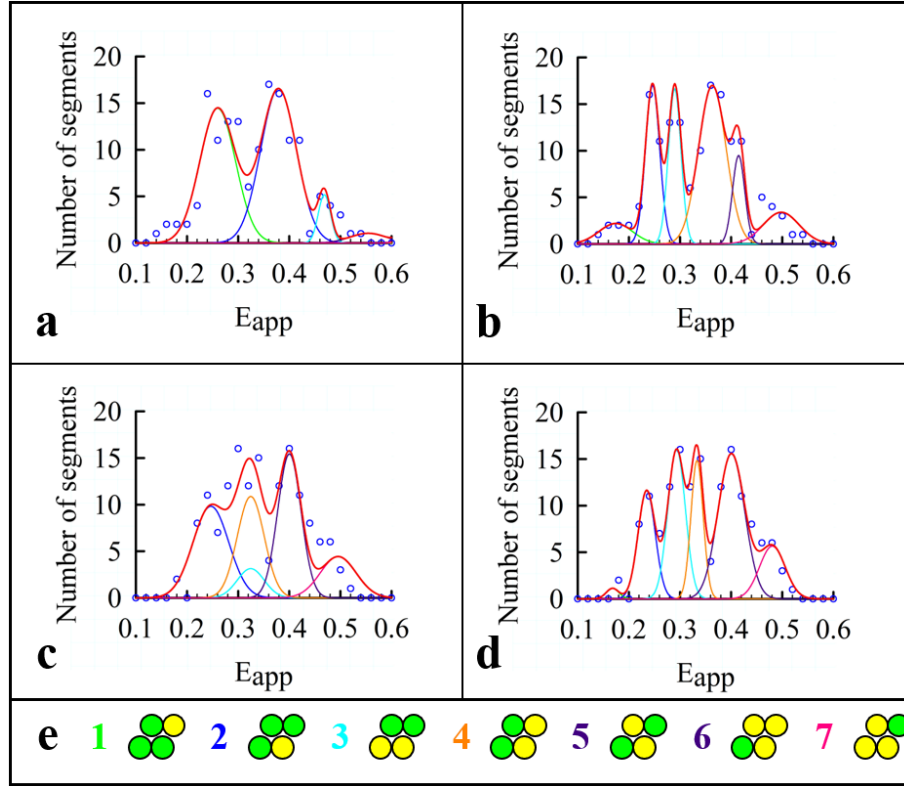


Figure S4. Comparison of meta-histogram fitting results using rhombus-shaped and general parallelogram-shaped tetramer models of cells co-expressing Ste2-GFP₂ and Ste2-YFP. Representative meta-histograms containing 150 peaks extracted from individual segment-level E_{app} histograms obtained from spectral images of Ste2 expressing cells in the (a, b) absence and (c, d) presence of ligand. Each data set was fit with two different models, and the fitting residual between data (blue circles) and model (solid red line) was minimized as described in Supplementary Methods section SM5. The geometrical parameters r_1/r_2 and α were allowed to vary while fitting the parallelogram model, but held fixed at $r_1/r_2=1$ and $\alpha = 60^\circ$ when fitting the rhombus model to the data. The number of parameters (f), used to calculate Res in Eq. (S6), was higher for the parallelogram model ($f = 15$) than for the rhombus model ($f = 11$). (a) The rhombus shape model fitted to a meta-histogram assembled from cells measured in the absence of ligand (expression level range, 57 to 157 molecules per μm^2). Best-fit value for the pairwise FRET efficiency was $E_p = 0.38$, with $Res = 6.3795$. (b) The general parallelogram model fitted to the same data in panel a. Best-fit parameters were as follows: $E_p = 0.30$, $r_1/r_2 = 0.92$ and $\alpha = 61.27^\circ$ with $Res = 1.7347$. (c) The rhombus model applied to the meta-histogram assembled from cells treated with α -factor ligand (expression level range, 48 to 140 molecules per μm^2). Best-fit value for the pairwise FRET efficiency was $E_p = 0.25$ with $Res = 7.7122$. (d) The general parallelogram model fitted to the same data in panel c. Best-fit parameter values were: $E_p = 0.27$, $r_1/r_2 = 0.96$ and $\alpha = 62.03^\circ$ with $Res = 1.2427$. (e) Visual representation of select configurations which have $E_{k,q}$ values corresponding to the various peaks found in the meta-histogram fittings under both tetrameric models.

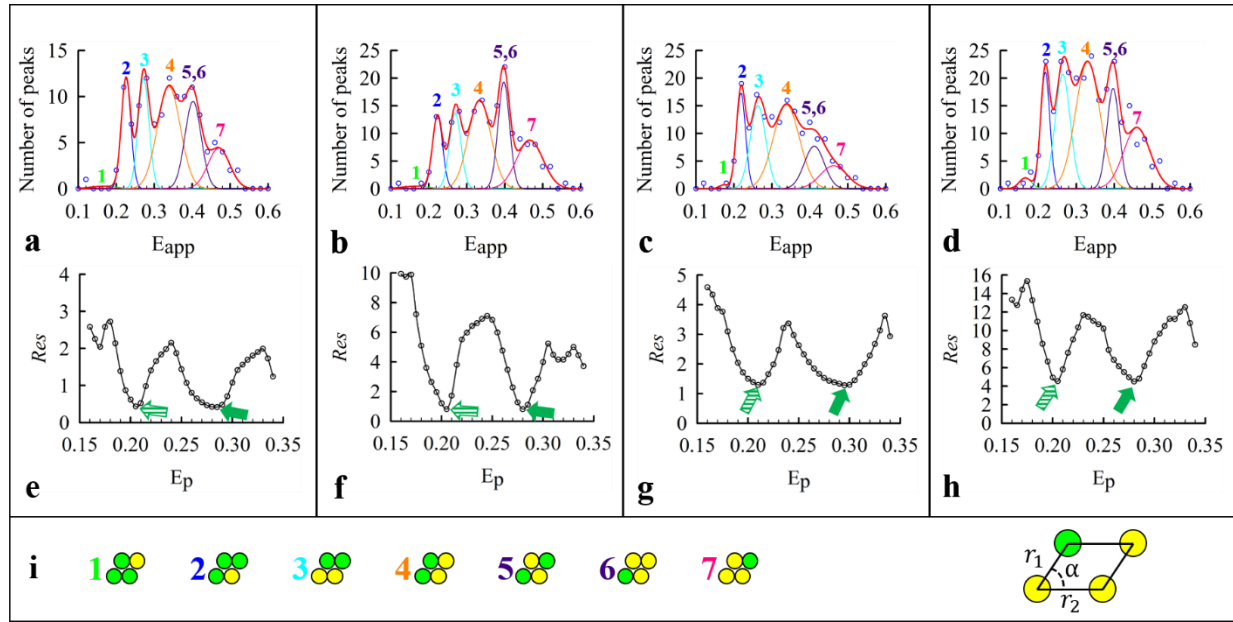


Figure S5. Typical histograms obtained from yeast (*S. cerevisiae*) cells co-expressing Ste2-GFP₂ and Ste2-YFP in the presence of α -factor at low receptor concentrations, and their analysis using an appropriate quaternary structure model. Experimental meta-histograms (empty blue circles) were obtained by collecting either single peaks (panels a and c) or two peaks (panels b and d) from each E_{app} histogram of the type shown in Figure 1. The meta-histograms were assembled for two different receptor concentration ranges: 53 to 134 receptors per μm^2 (panels a and b) and 53 to 144 receptors per μm^2 (panels c and d). Each meta-histogram was fit (solid red line) using a general parallelogram-shaped tetramer model, which consisted of a sum of seven Gaussians, whose centers correspond to the FRET values of particular FRET-productive configurations of donors and acceptors within a tetramer (see panel i). Positions of the seven meta-histogram peaks predicted by the model depend on only three parameters, E_p (i.e., the pairwise FRET efficiency), r_1/r_2 , and the angle α , which are used as adjustable parameters in the data fitting process. The minimization algorithm (see section 3.4 of the main text) began by fixing E_p to a value of 0.16, and then adjusting all other fitting parameters until the lowest possible reduced fitting residual, Res , (see Eq. S6) was obtained. The fitting process was then repeated several times for different values of E_p . A plot of the Res vs. E_p value (panels e-h) was computed for each corresponding meta-histogram placed in the panel above it. Note that there is a pair of complementary fits which give the same Res value for each meta-histogram (see Section SM5), indicated by the pair of arrows, and which are obtained by simply switching which sides (long or short) correspond to r_1 and r_2 in the model. Since complementary fits correspond to the same oligomer structure, only fitting parameters values corresponding to the minimum obtained for $r_1/r_2 < 1$ (indicated by solid color arrows) are retained for further analysis. The corresponding complementary fit to a minimum which is retained in subsequent analysis is indicated by a striped arrow of the same color. Best-fit parameter values and reduced residual, Res , corresponding to the minimum indicated by the solid color arrow were: $E_p = 0.285$, $r_1/r_2 = 0.93$, $\alpha = 66.38$, and $Res = 0.42$ for panels a and e; $E_p = 0.280$, $r_1/r_2 = 0.93$, $\alpha = 63.73$, and $Res = 0.81$ for b and f; $E_p = 0.295$, $r_1/r_2 = 0.93$, $\alpha = 67.33$, and $Res = 1.28$, for c and g; $E_p = 0.28$, $r_1/r_2 = 0.93$, $\alpha = 64.78$, and $Res = 4.49$ for d and h.

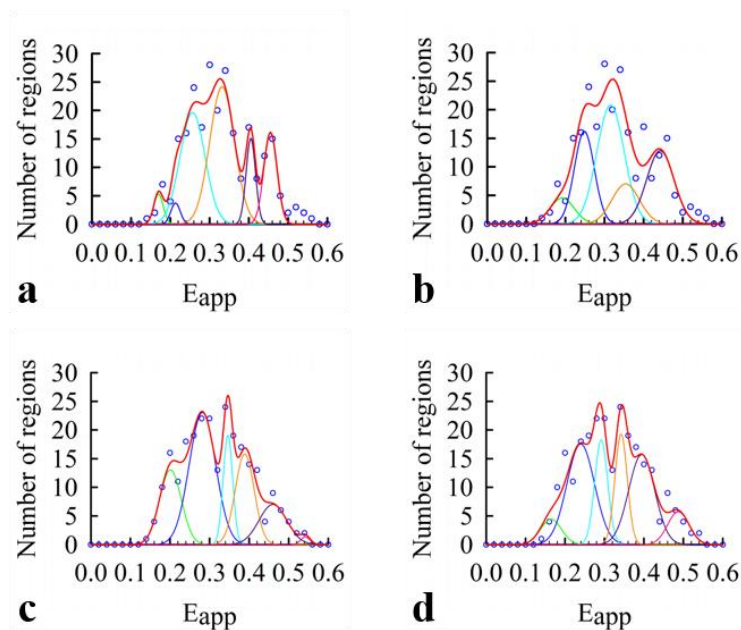


Figure S6. Testing uniqueness of meta-histogram fit. (a) The meta-histogram (blue symbols) and its fit using the parallelogram-shaped tetramer model (solid red line) resulted in a best-fit value for the r_1 distance located within the range of distances corresponding to peak 4 of Figure 3a, and the r_2 distance located within the range of distances corresponding to peak II of Figure 3b. The reduced residual (Eq. S6) is 9.71. (b) Same meta-histogram as in (a) fit by restricting the r_1 and r_2 distances to ranges corresponding to peak 1 and peak I from Figure 3a and 3b, respectively, while all other parameters used to generate the model were allowed to freely vary (Eq. S5). The minimized reduced residual was 16.24. (c and d) The process described in panel a and b was repeated for a meta-histogram whose best fit using the parallelogram-shaped tetramer model resulted in the r_1 distance falling into the range of distances corresponding to peak 1 of Figure 3a, and the distance r_2 located within peak I of Figure 3b. The reduced residuals were 4.13 and 6.85 for panels c and d, respectively.

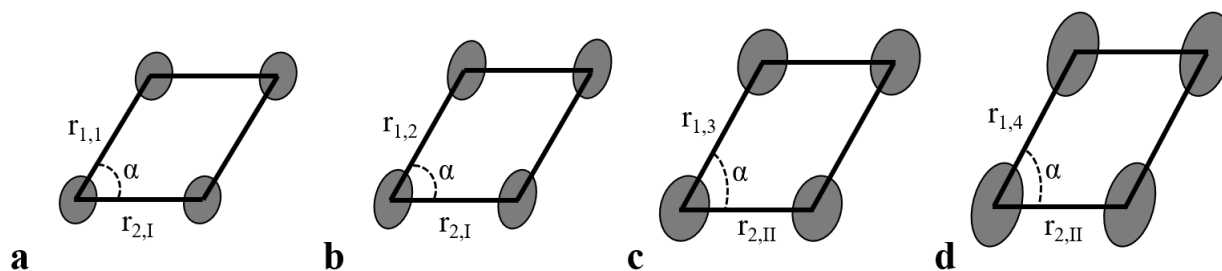


Figure S7. Schematic diagram representation of Ste2 receptor conformational substates. (a-d) Various conformations of the Ste2 quaternary structure, ranging from the basal inactive state to the fully active state. Grey circles represent Ste2 receptors. The lengths of each side of the parallelogram (r_1 and r_2) are labeled with a second index which indicates which conformation population (see Figure 3 in the main body of the paper) the side length is located within. For example, in the basal state, which is the smallest conformation shown in panel (a), the oligomeric distance termed $r_{1,1}$ is side length 1 located within the range of distances corresponding to conformation 1, and $r_{2,I}$ represents side length 2 located within the range of distances corresponding to conformation I. The second state, shown in (b), corresponds to a partially activated Ste2 receptor and gives a different r_1 distance ($r_{1,2}$), but the same r_2 distance when compared to panel a. Likewise, panel (c) shows another partially active quaternary conformational state with higher activity than that in panel b and which has a longer r_1 distance ($r_{1,3}$) and r_2 distance ($r_{2,II}$). The fully active state, shown in (d), is the largest of the conformations, with the longest r_1 distance ($r_{1,4}$) and also the longest r_2 distance ($r_{2,II}$). The growth of the circles in b, c, and d represent the flaring of the TM domains.

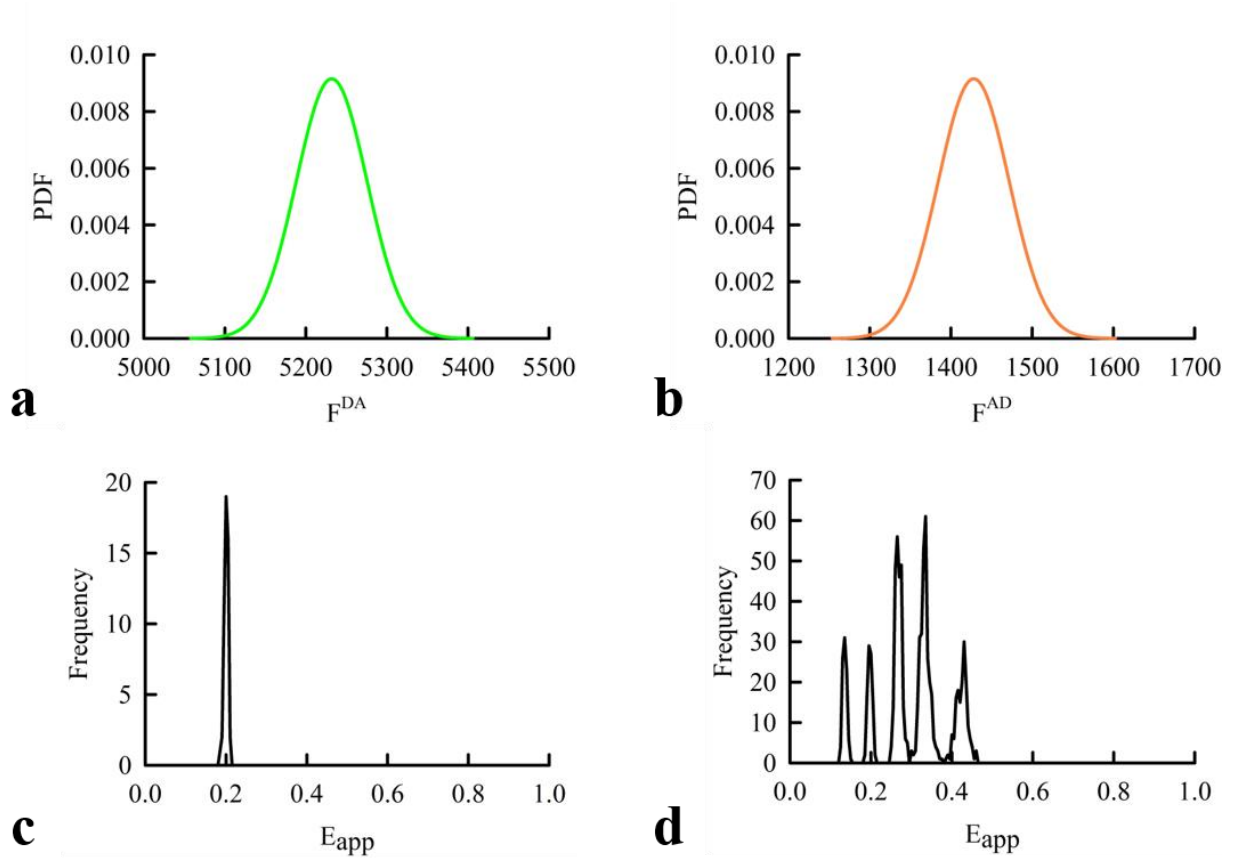


Figure S8. Computer-generated E_{app} histograms originating from image segments containing one FRET-ing rhombic tetramer per pixel. (a) F^{DA} and (b) F^{AD} probability distributions generated for configuration $q = 2$ of Table S1. Parameters used to describe the tetramer were $E_p = 0.2$, $r_1/r_2 = 1$, and $\alpha = 60$. The mean of each distribution was calculated by inserting the $E_{k,q}$ value of the given configuration into Eq. (S21) or (S22) and the distribution for the donor and acceptor signal calculated according to (S23), respectively. The standard deviation of the distributions was calculated using a fixed signal-to-noise ratio ($SNR = 50$), according to Eq. (S24). By choosing random F^{DA} and F^{AD} values from the distributions in panels a and b, a value for E_{app} was calculated according to Eq. (1). (c) E_{app} histogram resulting from repeating the process described in panels a and b for up to 1000 pixels when a single type of configuration, corresponding to $q = 2$ in Table S1, was placed in each pixel. (d) Meta-histogram assembled from pixels which could potentially contain any of the possible configurations of the tetramer; the specific configuration placed in a given pixel was randomly chosen based on a fixed donor-to-acceptor (D:A) ratio of 1.0 (see Eq. S20). This distribution closely simulates the experimentally obtained E_{app} histograms which were obtained from the pixel level E_{app} values in a single segment.

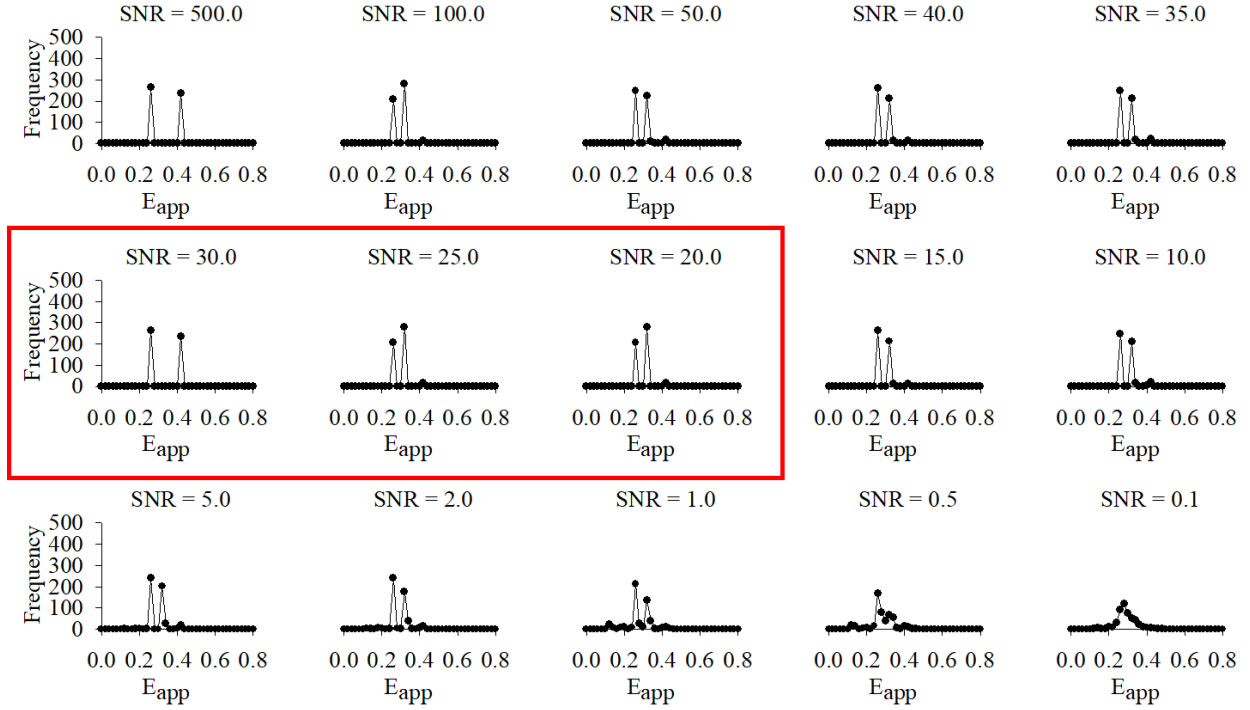


Figure S9. Meta-histograms constructed from computer-simulated E_{app} histograms generated for various signal-to-noise ratios. Computer-simulated E_{app} histograms were generated following the procedures described in Supplementary Methods section SM8. A single peak was extracted per computer-simulated E_{app} histogram (see Supplementary Methods section SM4). The E_{app} histograms for a particular meta-histogram were generated using a fixed signal-to-noise ratio (SNR); the value of SNR used for a given plot is displayed above the plot. The red box indicates the range of SNR levels present in the experimental meta-histograms.

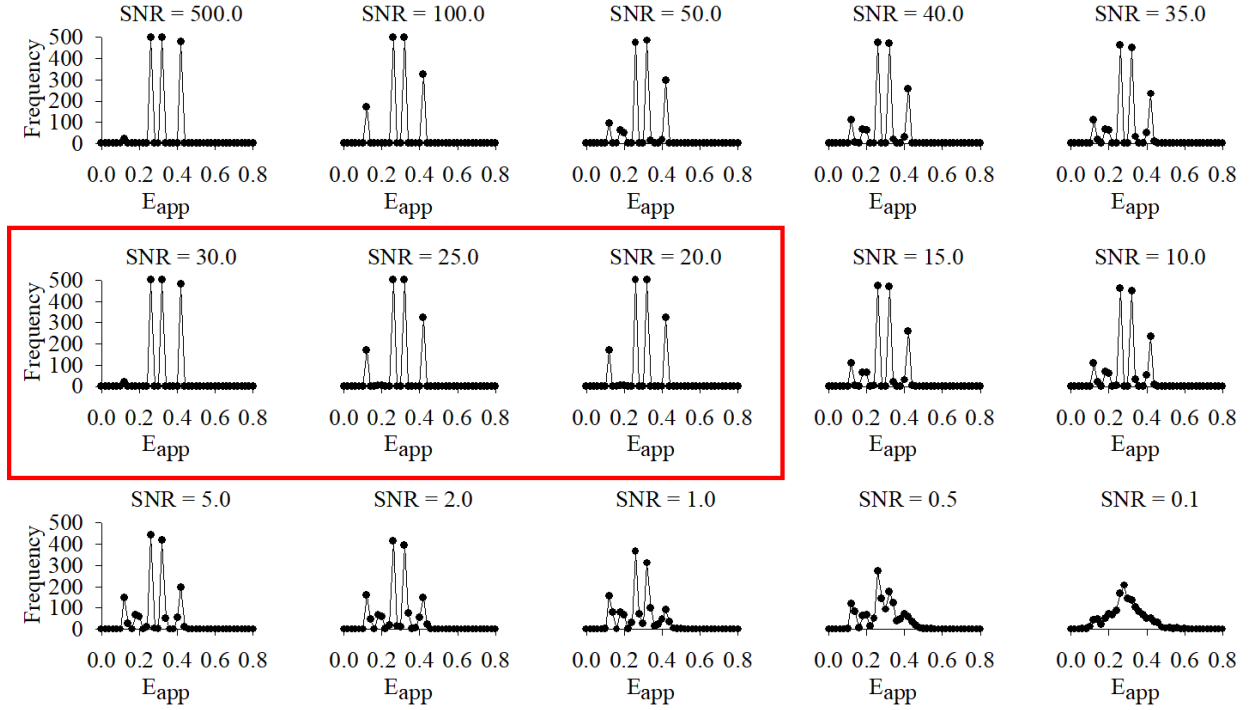


Figure S10. Meta-histograms constructed from computer-simulated E_{app} histograms generated at various signal-to-noise ratios. Computer-simulated E_{app} histograms were generated according to Supplementary Methods section SM8. Up to three peaks were extracted per computer-simulated E_{app} histogram (see Supplementary Methods section SM4). The E_{app} histograms for a particular meta-histogram were generated using a fixed signal-to-noise (SNR) ratio; the value of SNR used for a given plot is displayed above the plot. The red box indicates the range of SNR levels typically present in the experimental meta-histograms.

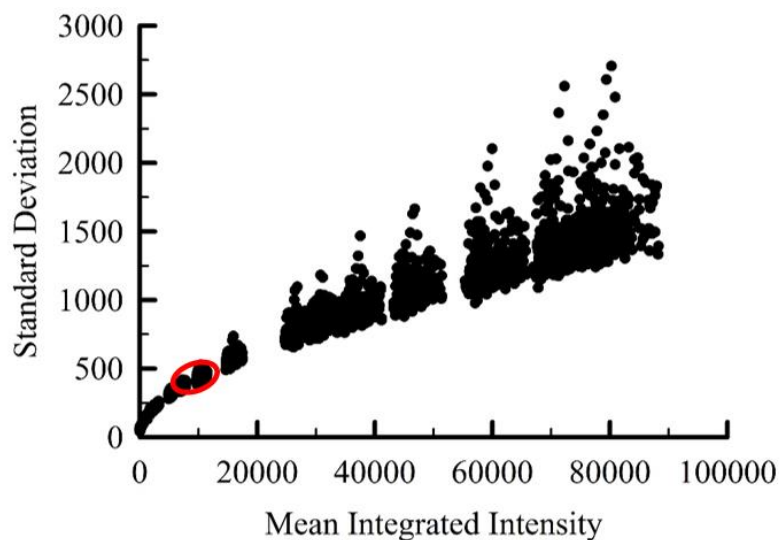


Figure S11. Characterization of EM-CCD camera noise for various light intensity levels. Micro-spectroscopic measurements were acquired while the EMCCD was illuminated with a constant light source; the measurements were repeated for a number of different light source levels. The signal was integrated over the wavelength channels corresponding to those of peak GFP₂ emission (495-550 nm). The mean and standard deviation of intensity distributions obtained from 20×20 pixel² regions were used to construct a plot of the standard deviation vs. corresponding mean intensity. The intensity values of donor plus acceptor fluorophores expressed at concentration levels which were used to construct the experimental meta-histograms were $10,000 \pm 5,000$; this intensity range is indicated by the red circle. The standard deviation of the intensity values detected for the constant light source in the intensity range within the red circle was ~300 to ~500, which corresponds to a calculated *SNR* of 20-30, according to Eq. (S24). Based on the results obtained for simulated meta-histograms generated using a *SNR* within this particular range (plots shown within red boxes of Figure S9 and S10) we can safely assume that noise does not generate artificial peaks in the experimental meta-histograms and that in fact the challenge is to reduce the noise such that the peaks are not erased or even obliterated.

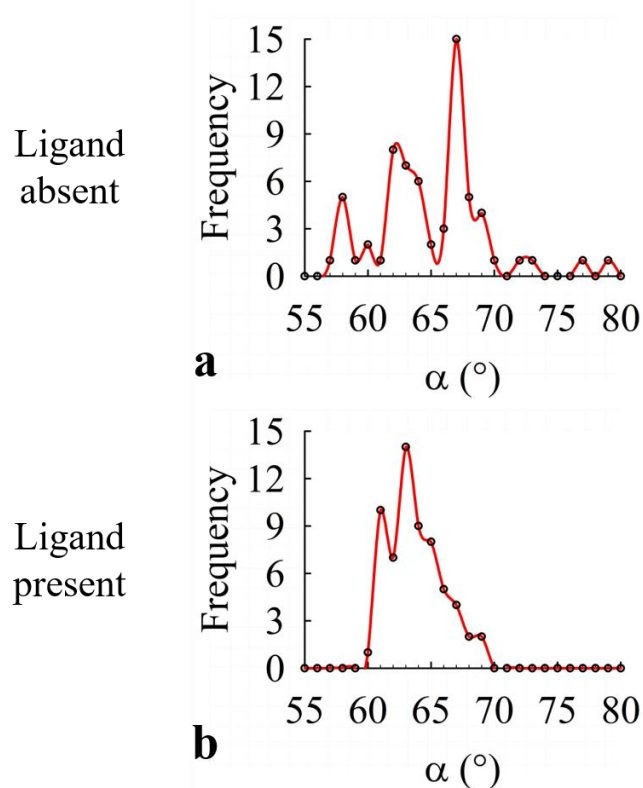
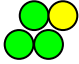
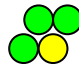
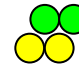
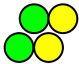

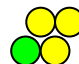
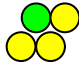


Figure S12. Histograms of frequencies of occurrence of the acute angle α of the general parallelogram-shaped tetramer. The distribution of α values was obtained from fitting the theoretical model (Figure 2) to the experimental meta-histograms for (a) untreated and (b) agonist-treated cells. The bin size was set to 1.0° for both histograms. The solid red line is drawn as a guide for the eye.

Table S1. Representative parallelogram tetramer configurations for each unique FRET efficiency per donor value ($E_{k,q}$).¹

Configuration	q	FRET Efficiency per Donor ($E_{k,q}$)
	1	$\frac{1}{3} \left[E_p + \frac{E_p \left(\frac{r_1}{r_2} \right)^6}{1 - E_p + E_p \left(\frac{r_1}{r_2} \right)^6} + \frac{E_p \left(\frac{r_1}{r_{d2}} \right)^6}{1 - E_p + E_p \left(\frac{r_1}{r_{d2}} \right)^6} \right]$
	2	$\frac{1}{3} \left[E_p + \frac{E_p \left(\frac{r_1}{r_2} \right)^6}{1 - E_p + E_p \left(\frac{r_1}{r_2} \right)^6} + \frac{E_p \left(\frac{r_1}{r_{d1}} \right)^6}{1 - E_p + E_p \left(\frac{r_1}{r_{d1}} \right)^6} \right]$
	3	$\frac{1}{2} \left\{ \frac{E_p + E_p \left(\frac{r_1}{r_{d1}} \right)^6}{1 - E_p + E_p \left[1 + \left(\frac{r_1}{r_{d1}} \right)^6 \right]} + \frac{E_p + E_p \left(\frac{r_1}{r_{d2}} \right)^6}{1 - E_p + E_p \left[1 + \left(\frac{r_1}{r_{d2}} \right)^6 \right]} \right\}$
	4	$\frac{1}{2} \left\{ \frac{E_p \left[\left(\frac{r_1}{r_2} \right)^6 + \left(\frac{r_1}{r_{d1}} \right)^6 \right]}{1 - E_p + E_p \left[\left(\frac{r_1}{r_2} \right)^6 + \left(\frac{r_1}{r_{d1}} \right)^6 \right]} + \frac{E_p \left[\left(\frac{r_1}{r_2} \right)^6 + \left(\frac{r_1}{r_{d2}} \right)^6 \right]}{1 - E_p + E_p \left[\left(\frac{r_1}{r_2} \right)^6 + \left(\frac{r_1}{r_{d2}} \right)^6 \right]} \right\}$
	5	$\frac{E_p + E_p \left(\frac{r_1}{r_2} \right)^6}{1 - E_p + E_p \left[1 + \left(\frac{r_1}{r_2} \right)^6 \right]}$
	6	$\frac{E_p + E_p \left(\frac{r_1}{r_2} \right)^6 + E_p \left(\frac{r_1}{r_{d2}} \right)^6}{1 - E_p + E_p \left[1 + \left(\frac{r_1}{r_2} \right)^6 + \left(\frac{r_1}{r_{d2}} \right)^6 \right]}$
	7	$\frac{E_p + E_p \left(\frac{r_1}{r_2} \right)^6 + E_p \left(\frac{r_1}{r_{d1}} \right)^6}{1 - E_p + E_p \left[1 + \left(\frac{r_1}{r_2} \right)^6 + \left(\frac{r_1}{r_{d1}} \right)^6 \right]}$

¹ The left-most column shows representative configurations from the seven potentially unique $E_{k,q}$ values (indexed by q in the second column) for the parallelogram tetramer geometrical shape. The position of each individual Gaussian used to simulate meta-histograms corresponds to the configuration of a particular row; the color of the numbers given in the second column match the color of the corresponding individual Gaussians shown for fitted meta-histograms in the manuscript (e.g., Figure 2 a-d), as well as the peaks found in Figure S4-S6. The third column displays the equations for computing the average FRET efficiency per donor for representative configurations of the general parallelogram-shaped tetramer model. It should be noted that $q = 5$ and 6 have near identical $E_{k,q}$ values, and for simplicity due to degeneracy, only $q = 5$ was used in fittings using this model.